Morphology-Dependent Electronic Properties in Cross-Linked (P3HT-*b*-P3MT) Block Copolymer Nanostructures

Mina Baghgar,[†,⊥] Austin M. Barnes,[†,⊥,⊗,*] Emily Pentzer,[‡,∥] Adam J. Wise,[§,#] Brenton A. G. Hammer,[‡,△] Todd Emrick,[‡] Anthony D. Dinsmore,[†] and Michael D. Barnes[†,§]

[†]Departments of Physics, [‡]Polymer Science and Engineering, and [§]Chemistry, University of Massachusetts, Amherst, Massachusetts 01003, United States. [⊥]M. Baghgar and A. M. Barnes contributed equally to this work. [⊗]Present address: Department of Chemistry, University of California, Santa Barbara, CA, USA. [∥]Present address: Department of Chemistry, Case Western Reserve University, Cleveland, OH, USA. [#]Present address: MacPherson, Inc., Chelmsford, MA, USA. [△]Present address: Max Planck Institute for Polymer Science, Mainz, Germany.

ABSTRACT Combined Kelvin probe force microscopy and wavelength-resolved photoluminescence measurements on individual pre- and post-cross-linked poly(3-hexylthiophene)-*b*-poly(3-methyl alcohol thiophene) (P3HT-*b*-P3MT) nanofibers have revealed striking differences in their optical and electronic properties driven by structural perturbation of the crystalline aggregate nanofiber structures after cross-linking. Chemical cross-linking from diblock copolymer P3HT-*b*-P3MT using a hexamethylene diisocyanate cross-linker produces a variety of morphologies including very small nanowires, nanofiber bundles, nanoribbons, and sheets, whose relative abundance can be controlled by reaction time and cross-linker concentration. While the different cross-linked morphologies have almost identical photophysical characteristics, KPFM measurements show that the surface potential contrast, related to the work function of the sample, depends sensitively on nanostructure morphology related to chain-packing disorder.

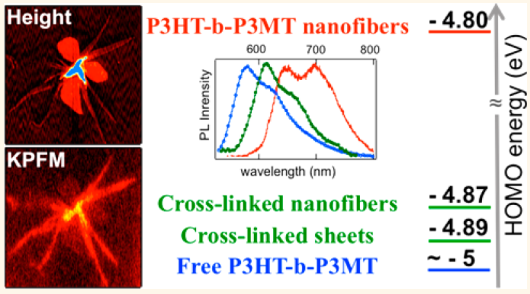

KEYWORDS: Kelvin probe · P3HT · morphology · cross-linking · work function · polarization · photoluminescence imaging and spectrum · electronic and optical properties

The search for high power conversion efficiencies in organic solar energy harvesting devices has produced breathtaking advances in new materials and processing techniques over the past several years.[1−5] One of the key device figures of merit is the open-circuit voltage, V_{oc}, which is directly related to electronic properties of donor and acceptor in the active layer, namely the difference between the donor highest occupied molecular orbital (HOMO) and the acceptor lowest unoccupied molecular orbital (LUMO) energy levels.[6] While considerable research effort has focused on the design and synthesis of new polymeric or small-molecule systems with adjustable HOMO or LUMO levels,[1,7] comparatively little is known about how different polymer chain packing motifs (*e.g.*, cofacial *vs* slip-stacked ordering) in the aggregate affect local work functions in optoelectronic devices. Motivated by recent theoretical studies on the effect of wave function overlap in adjacent polymer chains (and relationship to various geometrical parameters) on electronic properties of polythiophene aggregates,[8] we investigated the local surface potentials of P3HT nanoscale aggregates formed by chemical cross-linking *via* Kelvin probe force microscopy (KPFM).

While there is an extensive literature on photoluminescence probes of P3HT aggregate structure in films,[9−11] nanoparticles,[12−17] and nanofibers,[18−21] there is relatively limited experimental information on electronic properties correlated with different aggregate motifs with distinct H or J or H/J coupled systems.[22,23] Liscio and co-workers used KPFM to probe charge transport in graphene−P3HT blends,[24,25] as well as nanofiber-like structures formed from

* Address correspondence to mdbarnes@chem.umass.edu.

Received for review May 22, 2014 and accepted July 8, 2014.

Published online July 08, 2014
10.1021/nn502806d

dewetted P3HT films cast from chloroform,[26] to probe the modification of graphene electronic properties as influenced by P3HT additives. Ginger and co-workers have used both Kelvin probe and time-resolved electric force imaging techniques to probe the connection between electronic properties and local polymer morphology in solar cells[27−29] and photoinduced charge transport.[30] Here we address the question of how packing order (disorder) in isolated nanostructures of different morphology influences P3HT aggregate work function. To this end, we carried out KPFM measurements on P3HT nanofibers, which can yield precise spatial maps of HOMO energies that can then be correlated with structural order derived from spectroscopic measurements. We focus specifically on nanostructures made by chemical cross-linking of preformed crystalline aggregates of P3HT-*b*-P3MT diblock copolymers that yield small nanowires, nanofiber bundles, and clover-leaf-type nanosheets.[31]

We have recently shown that chemical cross-linking of preformed P3HT crystalline aggregates generates structurally robust nanostructures with tunable excitonic coupling and nanostructure morphology.[32] Such cross-linked materials in polymer active layers enhance overall device stability and performance over time. In this approach, we used a P3HT-*b*-P3MT diblock copolymer combined with a hexamethylene diisocyanate (HMD) cross-linking agent, which reacts with pendant hydroxyl groups on adjacent polymer chains. An interesting feature of the cross-linking of the P3HT-*b*-P3MT system with HMD is that depending on the initial aggregation state of the block copolymer, concentration of HMD, and reaction time, a wide variety of different cross-linked morphologies can be seen. Low HMD concentration and short reaction times favor small, more or less uniform cross-linked nanofiber structures, while higher HMD concentrations mostly produce branched structures, nanofiber bundles, and extended sheets.[31] The physical strain induced by the HMD cross-linker tends to disrupt the crystalline packing of the P3HT block aggregates, as evidenced by photoluminescence and transient absorption studies, indicating that most of the photophysical signatures of *ordered* aggregation in the P3HT (ultrafast intrachain exciton decay and interchain polaron absorption) are strongly diminished after HMD cross-linking.[32] For the present work, the interesting feature of this approach is that different nanoscale morphologies generated have distinct polarization characteristics, suggesting differences in post-cross-linked structural order implying different degrees of chain-packing disorder. As we show, the electronic properties—specifically changes in the frontier energy level location of the P3HT—depend on nanostructure morphology (ribbons *vs* extended sheets) even though their spectral properties are virtually identical. Thus, combining KPFM and photoluminescence studies provides access to otherwise hidden correlations between aggregation state and electronic properties.

RESULTS

Figure 1 shows the bright-field and polarization contrast images of a cross-linked bundle (a, b) and an extended sheet linked to a small array of nanowires (c, d). The polarization contrast images (b and d) were generated by raster-scanning a diffraction-limited excitation spot ($d \approx 1$ μm) across the sample while rotating the excitation polarization through 2π radians for each step. The *z*-value for each "pixel" of the polarization contrast image was determined by $M = (I_{max} - I_{min})/(I_{max} + I_{min})$, where I_{max} and I_{min} were the maximum and minimum photoluminescence intensity values for each step. The nanofiber bundle shows a fairly large variation of polarization contrast throughout the structure, with highest contrast (near unity) at the narrow neck (far right of the image). The discrete nanowires linked to an extended sheet in Figure 1d also show a high degree of polarization along almost its entire length, while the interior region of the sheet is almost completely unpolarized, indicating a random orientation of polymer chains.

Figure 1e shows photoluminescence spectra of isolated cross-linked nanostructures (green marker), along with emission spectra of isolated pre-cross-linked nanofibers (red markers) and solvated P3HT-*b*-P3MT polymers in chloroform (blue markers) for comparison. The solid-state PL spectra of isolated nanofibers and cross-linked nanostructures were obtained following drop-casting on a clean coverglass from chloroform/dichloromethane solution. Interestingly, all different individual cross-linked morphologies have virtually identical PL spectra. The emission spectra were properly modeled by a single vibronic progression consisting of three Gaussian functions with energy spacing varying over the range 170 (±5) meV. In this model, the progression offset (0−0 peak position), the amplitude of the 0−0 peak (and the higher vibronic sidebands), and transition bandwidths (fwhm of each Gaussians) were considered as adjustable parameters. Low molecular weight (<25 kDa) P3HTs are known to form nanofibers with extended chain conformation[20] with dominant interchain coupling as evidenced by 0−0/0−1 PL intensity ratios characteristic of H-type aggregates with a PL origin located at 640 nm. Cross-linking results in a dramatic change in nanofiber PL spectra; cross-linked aggregates (green line) resemble the PL spectrum of solvated P3HT-*b*-P3MT polymers (blue line) with 124 meV origin red-shift. This is due to cross-linking-induced alteration of molecular packing within the nanofibers, namely, perturbed interchain coupling and increased torsional disorder along the chain. The former results in a diminished interchain exciton coupling evidenced by an increase in the 0−0/0−1 PL intensity ratio from 0.87 to 1.69 and the absence of spectral dilation in the sideband.[23]

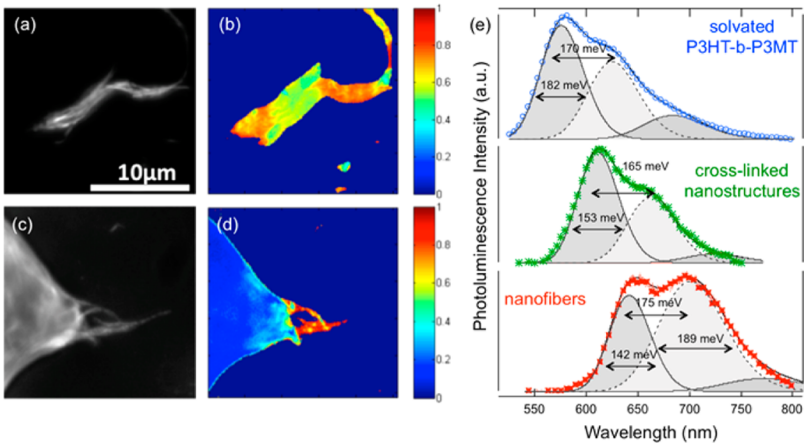

Figure 1. Bright-field (B/W) and polarization-contrast (color) optical images of a cross-linked nanofiber bundle (a, b) and nanofibers linked to an extended sheet (c, d). In the right set of images, the color-coding corresponds to polarization anisotropy: Red corresponds to a contrast parameter $M = 1$ (perfectly polarized), while blue corresponds to completely unpolarized ($M = 0$). (e) PL spectra of solvated P3HT-*b*-P3MT polymers (blue markers), isolated cross-linked nanostructures shown in a and c (green markers), and isolated crystalline nanofibers (red markers).

Figure 2 shows the AFM and KPFM images of well-separated P3HT-*b*-P3MT nanofibers (a and b) and cross-linked nanostructures (c and d) on a piranha acid treated cover glass. The color bar of KPFM images displays the relative surface potential value of nanostructures with respect to the cover glass, with a surface potential contrast (SPC) value of 0.6 ± 0.05 eV, and reveals a lower SPC value for cross-linked nanostructures compared with pre-cross-linked nanofibers. Nanofibers made from low molecular weight P3HT show minimal chain entanglement or folding; TEM imaging has shown 13 kDa nanofiber widths of 12−14 nm, in good agreement with polymer contour length for this molecular weight.[20] Because of their small transverse extent, these species allow for straightforward estimation of the microscope point-spread function (PSF). In AFM mode, transverse sections of pristine (non-cross-linked) P3HT-*b*-P3MT nanofibers show a Gaussian profile with a fwhm of ∼35 nm, in good agreement with expected convolution of a 15 nm step function (the nominal nanofiber width) and ∼20 nm tip radius. In SPC imaging, the transverse section is broadened, giving a fwhm in the SPC image of ∼75 nm. The topography image of cross-linked nanostructures, Figure 2c, depicts a variety of different nanostructured morphologies including single and bundled cross-linked nanofibers as well as "clover-leaf" sheets. Their corresponding KPFM image in Figure 2d shows spatial variation of SPC values along the NF axis in cross-linked fibers; higher SPC values are located in the center and lower SPC values are located near the edges. The KPFM image also shows that the "clover-leaf" sheets have a near-zero surface potential contrast.

Close inspection of branched cross-linked nanoribbons clearly shows SPC effects attributable to morphology and distinct from thickness artifacts known to influence SPC values of thin semiconducting samples

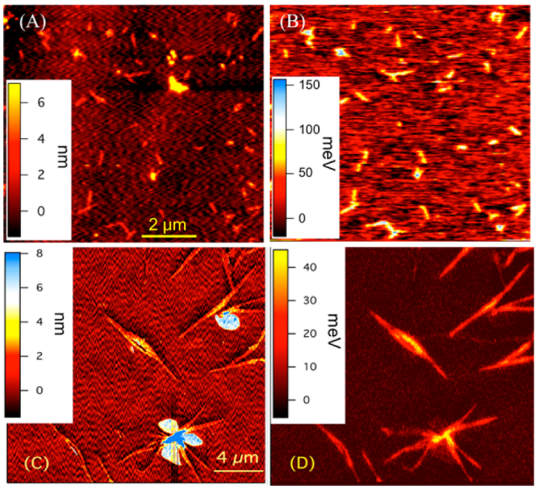

Figure 2. Surface height and SPC images of low molecular weight (13 kDa) P3HT-*b*-P3MT nanofibers (A, B) and cross-linked P3HT-P3MT nanostructures.

on dielectric substrates.[33] Figure 3 shows a closeup of the SPC image for this branched nanoribbon along with a section profile indicated by the solid yellow line segment. The surface height section (red triangles) shows that the nanoribbon thickness is almost identical for the two branches (4.2 nm), while the SPC differs by about 50% (+25 mV for the upper branch compared to 38 mV in the lower branch). Both branches have a lateral extent that is large compared to the point spread function of our microscope (75 nm), so this effect is clearly not associated with any lateral ($x-y$) artifactual averaging of sample and substrate SP signals.

Figure 4 shows a 2D scatter plot of surface potential and height of the two different cross-linked features, ribbons (red circle) and sheets (blue circles), and pre-cross-linked nanofibers (black circles). The scatter plot illustrates an overall decrease in the surface potential

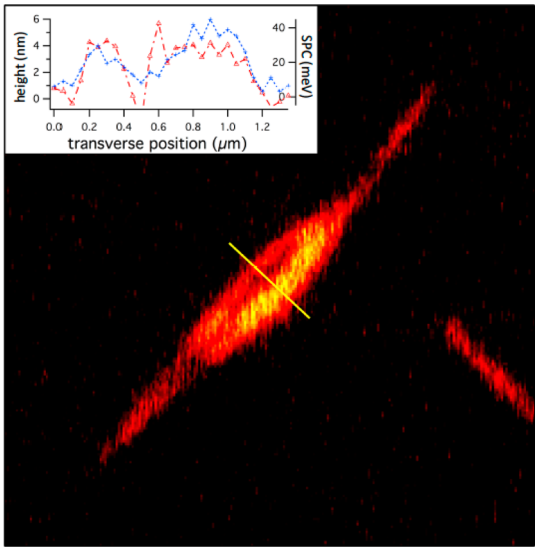

Figure 3. Closeup SPC image of branched cross-linked P3HT nanoribbon. Surface height (red) and SPC values (blue) are shown for the transverse section indicated by a yellow line. The nanoribbon height is almost identical for the two branches, while the SPC differs by ~50%.

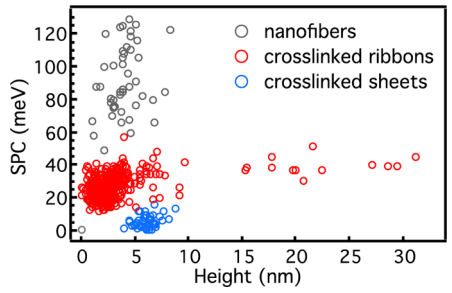

Figure 4. Scatter plots of measured SPC values relative to glass for P3HT-*b*-P3MT crystalline nanofibers (black circles), cross-linked nanoribbons (red circles), and extended cross-linked sheets (blue circles).

of nanostructures through the cross-linking process. The strongly diminished interchain coupling evidenced by wavelength- and time-resolved photoluminescence imaging[32] accompanies the reduction in the SPC value. Examining cross-linking-induced changes in the optical and electronic properties of P3HT nanofibers illustrates a full picture through which structural perturbation can be explained: interrupted lamellar spacing in cross-linked aggregates disrupts interchain coupling. This restricts the charge distributions mostly to individual extended chains in cross-linked nanostructures, in lieu of the two-dimensional (intermolecular and intramolecular) charge distribution seen in pre-cross-linked nanofibers. As a result, despite being in the aggregate, extended chains of cross-linked nanostructures do not effectively interact with each other and thus possess similar optical and electronic properties to isolated polymer chains. This is evident from their 30 nm blue-shifted PL origins (peaked at 610 nm) and reduced relative SPC value from 96 ± 30 meV in (non-cross-linked) nanofibers of similar molecular weight to 28 ± 8 meV in cross-linked nanoribbons. From KPFM on evaporated gold substrates, we determined the work function of our Pt−Si probes to be ~5.5 eV. This value for the probe work function is consistent with SPC measurements on the (borosilicate) glass substrates of *ca.* +600 meV, whose work function is also known from UPS to be 4.9−5.0 eV.[34] This places the nominal HOMO level of cross-linked nanoribbons at about −4.872 eV. This value falls within the range of reported HOMO energy level of solvated P3HT in toluene and chloroform (between −4.8 and −5.2) determined from cyclic voltammetry measurements.[35,36] This observation is consistent with recent work from Vanden Bout and co-workers on the morphology dependence on electronic properties of olighothiophene nanostructures,[37] where the decrease in the local contact potential of nanostructures with different morphologies is attributed to the increase in the amount of energetic disorder in the aggregate. They showed that subtle morphological changes in particle shape and molecular packing result in redistribution of charges within or between thiophene rings and accordingly change the electronic and optical properties. Correlating optical and electronic properties, they showed that the decrease in the SPC of nanostructures is associated with a decrease in interchain coupling strength. However, it is interesting to note that even though all the different cross-linked nanofeatures have identical optical properties and equivalent PL spectral shape and decay dynamics, the scatter plot reveals a morphology dependence of their surface potential, equivalently effective HOMO energy level. In fact, despite the spatial variation of SPC along the nanoribbons, their SPC distribution is distinguishable from that of cross-linked sheets. The average relative SPC of cross-linked nanosheets was determined to be about 25 meV less than that of cross-linked nanoribbons, which is independent of the surface height. The distinguishable electronic properties of different cross-linked morphologies may be due to subtle variation in their molecular packing densities that are not reflected in their photoluminescence properties. This indicates that their geometrical heterogeneity is correlated to heterogeneity on the molecular packing scale.

Recent theoretical work by Yamagata, Pochas, and Spano on wave function overlap[8] between neighboring chromophores provides insight into a plausible mechanism for these observations. In this work, the authors considered effects of exciton wave function overlap between adjacent polymer chains as a function of thiophene ring registration in staggered and eclipsed geometries in which one chain (considered as an 8T oligomer) is translated with respect to another, an effect that augments the usual Coulombic (through-space) excitonic coupling. The result is an oscillatory behavior in the transfer integrals for adjacent HOMO

and LUMO wave functions (t_{HOMO}, t_{LUMO}) as a function of longitudinal shift; the value of t_{HOMO} relates directly to the work function of the nanostructure. For the extended cross-linked P3HT sheets, the polarization contrast image shows almost complete depolarization, implying a high degree of chain-packing disorder. Within the wave function overlap (WFO) transfer integral picture, the net effect is presumably to average over all shifts and orientations, thus reducing the overall magnitude of the effect. Future work on KPFM imaging of nanofibers of different molecular weight (which show qualitatively different exciton coupling) may help in definitive assignment of the mechanism for morphology-dependent work functions observed in this interesting class of photoactive materials.

CONCLUSIONS

KPFM measurements have revealed an interesting dependence of surface potential contrast with P3HT nanostructure morphology. In comparing SPC for diblock copolymer crystalline nanofibers and cross-linked structures of different morphology, we found that the work function of crystalline nanofibers increases by 70 meV (4.80 to 4.87 eV) upon cross-linking. Correlating optical and electronic properties of nanostructures before and after cross-linking indicates that the cross-link-induced molecular structure perturbation reduces interchain coupling strength and increases torsional disorder. The SPC of cross-linked structures depends on morphology as well as spatial location within a given nanostructure, providing additional insight into the mechanism of nanostructure growth and internal microstructure after cross-linking. Polarized luminescence studies combined with models of exciton coupling with slip-stacked P3HT suggest that the physical origin of morphological dependence in SPC derives from thiophene ring mis-alignment in lamellar stacks that perturb the HOMO energy.

METHODS/EXPERIMENTAL

Kelvin probe force microscopy is a scanning probe technique that measures the local surface potential contrast between a metalized cantilever tip and sample.[38−41] The tip−sample interaction generates a contact (surface) potential difference approximately given by $V \approx (1/e)(\phi_1 - \phi_2)$, where e is the charge constant and ϕ_1, ϕ_2 are the work functions of the tip and sample, respectively.[38] In our imaging mode, the SPC is measured by applying an ac voltage and dc offset to the cantilever tip to generate an oscillating electrostatic force between the tip and the sample. This feedback loop provides a dc offset potential to match the surface potential that minimizes the electrostatic interaction between the tip and sample; it is the dc input that is recorded as the measured surface potential contrast. KPFM imaging can yield quantitative information on the energy location of the sample's HOMO if the work function of the tip is known.[25,41,42] The most convenient way to achieve this is to image a sample with a well-characterized work function such as single-layer graphene (ϕ = 4.77 eV),[43] multilayer graphene,[43,44] or a metal surface such as gold.[38]

KPFM measurements were made with an Asylum Research AFM (model MFP-3D); MFP3D software was used to run the Kelvin probe module. All measurements were made in non-contact tapping mode, under ambient atmospheric conditions. The AFM probes were platinum/iridium-coated silicon (ANSCM-PT) used as supplied by App Nano. As typical for electrostatic force measurements, KPFM imaging employs trace and retrace line scans: the first obtains topography information; then a retrace over the same line scan maintaining a constant height above the sample surface gives SPC information. All imaging experiments used a 50 nm initial lift height (adjusted in the Nap mode settings in the MFP3D software); depending on the overlap between the trace and retrace scan lines of the surface potential image, the lift height was reduced to about 10−20 nm above the van der Waals attractive regime (typically 10−30 nm from the substrate). Scan rates were lowered to ∼0.2 Hz to improve the resolution of the CPD images by allowing the cantilever to settle on an accurate surface potential value.

Crystalline P3HT-*b*-P3MT diblock copolymer nanofibers prepared from low molecular weight (13 kDa, 1.2 PDI) with high regioregularity (∼98%) were made by adding dichloromethane (DCM) to the well-dissolved P3HT in chloroform (CF) (2 mg/mL) for final 7:1 volume ratios of DCM to CF and left at 0 °C in the dark overnight.[31] The crystalline core of the diblock copolymer nanofibers is composed mostly of the P3HT block, where the P3MT block mostly decorates the nanofiber exterior.[31,32] Cross-linked P3HT-*b*-P3MT nanostructures were fabricated from diblock copolymer nanofibers by adding freshly distilled anhydrous triethylamine (1 mL) and hexamethylene diisocyanate (0.1 mL) to the nanofiber solution and stirring it at room temperature in the dark for 12 h.[31] The cross-linked nanostructures in mixed CF/DCM were used directly or isolated by centrifugation at 1000 rpm for 10 min followed by removal of the solvent by pipet and resuspending them in the desired solvent.

Conflict of Interest: The authors declare no competing financial interest.

Acknowledgment. A.M.B. acknowledges support from the NSF-funded MRSEC on Polymers (DMR-0820506) at UMass Amherst. T.E. acknowledges support from NSF-CHE 1152360 for the synthesis of functional polymers. M.B., A.J.W., and M.D.B. acknowledge support from U.S. Department of Energy under Grant No. DE-FG02-05ER15695 (Program Manager: Larry Rahn).

REFERENCES AND NOTES

1. Thompson, B. C.; Frechet, J. M. J. Organic Photovoltaics - Polymer-Fullerene Composite Solar Cells. *Angew. Chem., Int. Ed.* **2008**, *47*, 58–77.
2. Gunes, S.; Neugebauer, H.; Sariciftci, N. S. Conjugated Polymer-Based Organic Solar Cells. *Chem. Rev.* **2007**, *107*, 1324–1338.
3. Hoppe, H.; Sariciftci, N. S. Organic Solar Cells: An Overview. *J. Mater. Res.* **2004**, *19*, 1924–1945.
4. Scharber, M. C.; Sariciftci, N. S. Efficiency of Bulk-Heterojunction Organic Solar Cells. *Prog. Polym. Sci.* **2013**, *38*, 1929–1940.
5. Darling, S. B.; You, F. Q. The Case for Organic Photovoltaics. *RSC Adv.* **2013**, *3*, 17633–17648.
6. Scharber, M. C.; Wuhlbacher, D.; Koppe, M.; Denk, P.; Waldauf, C.; Heeger, A. J.; Brabec, C. L. Design Rules for Donors in Bulk-Heterojunction Solar Cells - Towards 10% Energy-Conversion Efficiency. *Adv. Mater.* **2006**, *18*, 789–794.
7. Brabec, C. J.; Gowrisanker, S.; Halls, J. J. M.; Laird, D.; Jia, S. J.; Williams, S. P. Polymer-Fullerene Bulk-Heterojunction Solar Cells. *Adv. Mater.* **2010**, *22*, 3839–3856.
8. Yamagata, H.; Pochas, C. M.; Spano, F. C. Designing J- and H-Aggregates through Wave Function Overlap Engineering: Applications to Poly(3-hexylthiophene). *J. Phys. Chem. B* **2012**, *116*, 14494–14503.

9. Clark, J.; Chang, J. F.; Spano, F. C.; Friend, R. H.; Silva, C. Determining Exciton Bandwidth and Film Microstructure in Polythiophene Films Using Linear Absorption Spectroscopy. *Appl. Phys. Lett.* **2009**, *94*, 163306.
10. Clark, J.; Silva, C.; Friend, R. H. Spano, F. C. Role of Intermolecular Coupling in the Photophysics of Disordered Organic Semiconductors: Aggregate Emission in Regioregular Polythiophene. *Phys. Rev. Lett.* **2007**, *98*, Article No. 206406.
11. Spano, F. C.; Clark, J.; Silva, C.; Friend, R. H. Determining Exciton Coherence from the Photoluminescence Spectral Line Shape in Poly(3-hexylthiophene) Thin Films. *J. Chem. Phys.* **2009**, *130*, 074904.
12. Labastide, J. A.; Baghgar, M.; Dujovne, I.; Yang, Y. P.; Dinsmore, A. D.; Sumpter, B. G.; Venkataraman, D.; Barnes, M. D. Polymer Nanoparticle Super Lattices for Organic Photovoltaic Applications. *J. Phys. Chem. Lett.* **2011**, *2*, 3085–3091.
13. Labastide, J. A.; Baghgar, M.; Dujovne, I.; Venkatraman, B. H.; Ramsdell, D. C.; Venkataraman, D.; Barnes, M. D. Time- and Polarization-Resolved Photoluminescence of Individual Semicrystalline Polythiophene (P3HT) Nanoparticles. *J. Phys. Chem. Lett.* **2011**, *2*, 2089–2093.
14. Nagarjuna, G.; Baghgar, M.; Labastide, J. A.; Algaier, D. D.; Barnes, M. D.; Venkataraman, D. Tuning Aggregation of Poly(3-hexylthiophene) within Nanoparticles. *ACS Nano* **2012**, *6*, 10750–10758.
15. Vogelsang, J.; Adachi, T.; Brazard, J.; Bout, D. A. V.; Barbara, P. F. Self-Assembly of Highly Ordered Conjugated Polymer Aggregates with Long-Range Energy Transfer. *Nat. Mater.* **2011**, *10*, 942–946.
16. Moule, A. J.; Allard, S.; Kronenberg, N. M.; Tsami, A.; Scherf, U.; Meerholz, K. Effect of Polymer Nanoparticle Formation on the Efficiency of Polythiophene Based "Bulk-Heterojunction" Solar Cells. *J. Phys. Chem. C* **2008**, *112*, 12583–12589.
17. Tenery, D.; Gesquiere, A. J. Interplay between Fluorescence and Morphology in Composite MEH-PPV/PCBM Nanoparticles Studied at the Single Particle Level. *Chem. Phys.* **2009**, *365*, 138–143.
18. Niles, E. T.; Roehling, J. D.; Yamagata, H.; Wise, A. J.; Spano, F. C.; Moule, A. J.; Grey, J. K. J-Aggregate Behavior in Poly-3-hexylthiophene Nanofibers. *J. Phys. Chem. Lett.* **2012**, *3*, 259–263.
19. Labastide, J. A.; Baghgar, M.; McKenna, A.; Barnes, M. D. Time- and Polarization-Resolved Photoluminescence Decay from Isolated Polythiophene (P3ht) Nanofibers. *J. Phys. Chem. C* **2012**, *116*, 23803–23811.
20. Baghgar, M.; Labastide, J.; Bokel, F.; Dujovne, I.; McKenna, A.; Barnes, A. M.; Pentzer, E.; Emrick, T.; Hayward, R.; Barnes, M. D. Probing Inter- and Intrachain Exciton Coupling in Isolated Poly(3-hexylthiophene) Nanofibers: Effect of Solvation and Regioregularity. *J. Phys. Chem. Lett.* **2012**, *3*, 1674–1679.
21. Barnes, M. D.; Baghar, M. Optical Probes of Chain Packing Structure and Exciton Dynamics in Polythiophene Films, Composites, and Nanostructures. *J. Polym. Sci. Polym. Phys.* **2012**, *50*, 1121–1129.
22. Yamagata, H.; Spano, F. C. Interplay between Intrachain and Interchain Interactions in Semiconducting Polymer Assemblies: The HJ-Aggregate Model. *J. Chem. Phys.* **2012**, *136*, 184901.
23. Spano, F. C. The Spectral Signatures of Frenkel Polarons in H- and J-Aggregates. *Acc. Chem. Res.* **2010**, *43*, 429–439.
24. Liscio, A.; Veronese, G. P.; Treossi, E.; Suriano, F.; Rossella, F.; Bellani, V.; Rizzoli, R.; Samori, P.; Palermo, V. Charge Transport in Graphene-Polythiophene Blends as Studied by Kelvin Probe Force Microscopy and Transistor Characterization. *J. Mater. Chem.* **2011**, *21*, 2924–2931.
25. Liscio, A.; Palermo, V.; Samori, P. Nanoscale Quantitative Measurement of the Potential of Charged Nanostructures by Electrostatic and Kelvin Probe Force Microscopy: Unraveling Electronic Processes in Complex Materials. *Acc. Chem. Res.* **2010**, *43*, 541–550.
26. Liscio, A.; Palermo, V.; Samori, P. Probing Local Surface Potential of Quasi-One-Dimensional Systems: A KPFM Study of P3ht Nanofibers. *Adv. Funct Mater.* **2008**, *18*, 907–914.
27. Giridharagopal, R.; Shao, G. Z.; Groves, C.; Ginger, D. S. New SPM Techniques for Analyzing Opv Materials. *Mater. Today.* **2010**, *13*, 50–56.
28. Coffey, D. C.; Reid, O. G.; Rodovsky, D. B.; Bartholomew, G. P.; Ginger, D. S. Mapping Local Photocurrents in Polymer/Fullerene Solar Cells with Photoconductive Atomic Force Microscopy. *Nano Lett.* **2007**, *7*, 738–744.
29. Coffey, D. C.; Ginger, D. S. Time-Resolved Electrostatic Force Microscopy of Polymer Solar Cells. *Nat. Mater.* **2006**, *5*, 735–740.
30. Noone, K. M.; Subramaniyan, S.; Zhang, Q. F.; Cao, G. Z.; Jenekhe, S. A.; Ginger, D. S. Photoinduced Charge Transfer and Polaron Dynamics in Polymer and Hybrid Photovoltaic Thin Films: Organic vs. Inorganic Acceptors. *J. Phys. Chem. C* **2011**, *115*, 24403–24410.
31. Hammer, B. A. G.; Bokel, F. A.; Hayward, R. C.; Emrick, T. Cross-Linked Conjugated Polymer Fibrils: Robust Nanowires from Functional Polythiophene Diblock Copolymers. *Chem. Mater.* **2011**, *23*, 4250–4256.
32. Baghgar, M.; Pentzer, E.; Wise, A. J.; Labastide, J. A.; Emrick, T.; Barnes, M. D. Cross-Linked Functionalized Poly(3-hexylthiophene) Nanofibers with Tunable Excitonic Coupling. *ACS Nano* **2013**, *7*, 8917–8923.
33. Liscio, A.; Palermo, V.; Fenwick, O.; Braun, S.; Mullen, K.; Fahlman, M.; Cacialli, F.; Samori, P. Local Surface Potential of Pi-Conjugated Nanostructures by Kelvin Probe Force Microscopy: Effect of the Sampling Depth. *Small* **2011**, *7*, 634–639.
34. Muray, J. J. Surface Conductivity of Borosilicate Glass. *J. Appl. Phys.* **1962**, *33*, 1525–1527.
35. Al-Ibrahim, M.; Roth, H. K.; Zhokhavets, U.; Gobsch, G.; Sensfuss, S. Flexible Large Area Polymer Solar Cells Based on Poly(3-hexylthiophene)/Fullerene. *Sol. Energy Mater. Sol. Cells* **2005**, *85*, 13–20.
36. Kim, J. B.; Allen, K.; Oh, S. J.; Lee, S.; Toney, M. F.; Kim, Y. S.; Kagan, C. R.; Nuckolls, C.; Loo, Y.-L. Small-Molecule Thiophene-C60 Dyads as Compatibilizers in Inverted Polymer Solar Cells. *Chem. Mater.* **2010**, *22*, 5762–5773.
37. Ostrowski, D. P.; Lytwak, L. A.; Mejia, M. L.; Stevenson, K. J.; Holliday, B. J.; Vanden Bout, D. A. The Effects of Aggregation on Electronic and Optical Properties of Oligothiophene Particles. *ACS Nano* **2012**, *6*, 5507–5513.
38. Nonnenmacher, M.; Oboyle, M. P.; Wickramasinghe, H. K. Kelvin Probe Force Microscopy. *Appl. Phys. Lett.* **1991**, *58*, 2921–2923.
39. Girard, P. Electrostatic Force Microscopy: Principles and Some Applications to Semiconductors. *Nanotechnology* **2001**, *12*, 485–490.
40. Umeda, K.; Kobayashi, K.; Ishida, K.; Hotta, S.; Yamada, H.; Matsushige, K. Surface Potential Measurement of Oligothiophene Ultrathin Films by Kelvin Probe Force Microscopy. *Jpn. J. Appl. Phys. 1* **2001**, *40*, 4381–4383.
41. Lei, C. H.; Das, A.; Elliott, M.; Macdonald, J. E. Quantitative Electrostatic Force Microscopy-Phase Measurements. *Nanotechnology* **2004**, *15*, 627–634.
42. Cuenat, A.; Muniz-Piniella, A.; Munoz-Rojo, M.; Tsoi, W. C.; Murphy, C. E. Quantitative Nanoscale Surface Voltage Measurement on Organic Semiconductor Blends. *Nanotechnology* **2012**, *23*, 045703.
43. Yu, Y. J.; Zhao, Y.; Ryu, S.; Brus, L. E.; Kim, K. S.; Kim, P. Tuning the Graphene Work Function by Electric Field Effect. *Nano Lett.* **2009**, *9*, 3430–3434.
44. Zhou, Y. H.; Fuentes-Hernandez, C.; Shim, J.; Meyer, J.; Giordano, A. J.; Li, H.; Winget, P.; Papadopoulos, T.; Cheun, H.; Kim, J.; Fenoll, M.; Dindar, A.; Haske, W.; Najafabadi, E.; Khan, T. M.; Sojoudi, H.; Barlow, S.; Graham, S.; Bredas, J. L.; Marder, S. R.; Kahn, A.; Kippelen, B. A Universal Method to Produce Low-Work Function Electrodes for Organic Electronics. *Science* **2012**, *336*, 327–332.